Generation of NNBN via Photolysis of $B(N_3)_3$ in Low-Temperature Argon Matrices: IR Spectra and ab Initio Calculations

Ismail A. Al-Jihad, Bing Liu, Christopher J. Linnen, and Julanna V. Gilbert*

Department of Chemistry & Biochemistry, University of Denver, Denver, Colorado 80208

Received: February 24, 1998; In Final Form: May 12, 1998

$B(N_3)_3$ was isolated in a low-temperature argon matrix and its FTIR spectrum measured. The spectrum was consistent with the known gas-phase spectrum, and splitting due to the natural abundances of ^{10}B and ^{11}B was observed. Upon UV photolysis, new peaks at 2100, 1861, and 1803 cm^{-1} assigned to the linear molecule NNBN appeared as the $B(N_3)_3$ peaks decayed. Geometry optimizations and calculations of the ground-state frequencies for ^{10}B and ^{11}B isotopomers $B(N_3)_3$ [MP2/6-31G(d)] and NNBN [CCSD(T)/6-311G*] are reported, and the frequencies are compared to those observed in the IR spectra. The photolytic decomposition mechanism of $B(N_3)_3$ is discussed.

Introduction

Boron triazide, $B(N_3)_3$, a nearly planar trigonal molecule, decomposes spontaneously to form N_2-rich hexagonal BN films.[1] Upon irradiation with broad-band UV light, the gaseous dissociation was observed to occur more rapidly, and the films produced displayed both hexagonal and cubic characteristics. A combination of hexagonal and cubic crystal structures was also generated when gas-phase $B(N_3)_3$ was allowed to decompose with mild heating (50 °C). These results suggest that there are two paths by which the decomposition can proceed: a room-temperature path resulting in hexagonal BN films and an energetic path producing cubic BN which is made accessible by adding energy in the form of heat or light.

Studies of cubic boron nitride (c-BN) are motivated by its potential application as a hard protective coating (it is second in hardness only to diamond and is less reactive than diamond) and because of its characteristics as a semiconductor material.[2] It has a wide band gap (in excess of 6.33 eV) and high thermal conductivity and can be doped to be either a p- or n-type material.[3] Existing industrial methods generate c-BN films via reactions between compounds that are stable at room temperature, requiring the input of significant amounts of energy (for example with plasma discharges, high heat, or pulsed lasers) to initiate the process.[4−6] Since $B(N_3)_3$ is synthesized and decomposes to form BN films without requiring excessive energy input, problems associated with film damage caused by differential cooling or impact of high-energy species with the film are avoided.

The $B(N_3)_3$ system is also of particular interest to chemists because of the simplicity of the decomposition system, where only boron- and/or nitrogen-containing species are produced. Thus, the system is amenable to detailed studies of film formation including the identification of the intermediates involved. This has generally not been possible with "traditional" systems because the detection of intermediates is complicated or rendered impossible by the presence of the many different energetic species in the typical film deposition apparatus.

Some information regarding the photolytic decomposition of $B(N_3)_3$ is available from the gas-phase studies[1] and from the photolytic processes of other covalent azides. The UV absorption spectrum of gaseous $B(N_3)_3$ consists of a single structureless feature at 230 nm, indicative of a dissociative electronic transition. UV photolysis of 0.3 Torr of gaseous $B(N_3)_3$ caused the pressure to increase by 0.6 Torr; thus, 3 equiv of gaseous product was generated for every 1 equiv of $B(N_3)_3$(g). Photolysis of $B(N_3)_3$ is predicted to be similar to other covalent azides and form diatomic nitrogen. For example, for the XN_3 species (X = H, Cl, F), photolysis breaks the $XN-N_2$ bond of the azide group and generates XN and N_2 in high yields.[7−9] Using this information and the pressure data from the $B(N_3)_3$ gas-phase decomposition studies, the following process was proposed:[1]

$$B(N_3)_3(g) + h\nu \rightarrow BN_3(s) + 3N_2(g) \qquad (1)$$

The nature of the intermediate species BN_3 is to be addressed in the work reported here.

To identify the photolytic intermediate, $B(N_3)_3$ was isolated in a low-temperature argon matrix and then photolyzed. Since the progress of the photolysis was monitored by following changes in the infrared spectrum, the infrared spectrum of the matrix-isolated $B(N_3)_3$ is compared to the previously reported gas-phase spectrum, and infrared features assigned to the ^{10}B isotopomer are identified. Photolysis of the $B(N_3)_3$/Ar matrix generated the linear molecule NNBN, a molecule that has been previously isolated and identified in low-temperature argon and nitrogen matrices as a product in B + N_2 reactions.[10,11]

Experimental Section

Boron triazide is prepared at room temperature in the gas phase by mixing BCl_3 and HN_3 in a 1:3 ratio. For these experiments, a few Torr of pure BCl_3 (Matheson) was admitted to a 5 L Pyrex gas bulb and diluted to 1% with argon. HN_3 was synthesized via the NaN_3 plus excess steric acid reaction as described in ref 12, and a 1% mixture of HN_3 in argon was prepared in a second 5 L Pyrex gas bulb. It is noted here that HN_3 is an explosive and toxic substance and must be synthesized and handled with care. Because boron triazide is not a stable compound, a gas-phase synthesis manifold (shown in Figure 1) was coupled to the cryostat (RMC model 22). The two Pyrex bulbs, one containing a 1% mixture of BCl_3 in argon and the other containing a 1% mixture of HN_3 in argon, were attached

S1089-5639(98)01268-7 CCC: $15.00
Published on Web 07/10/1998

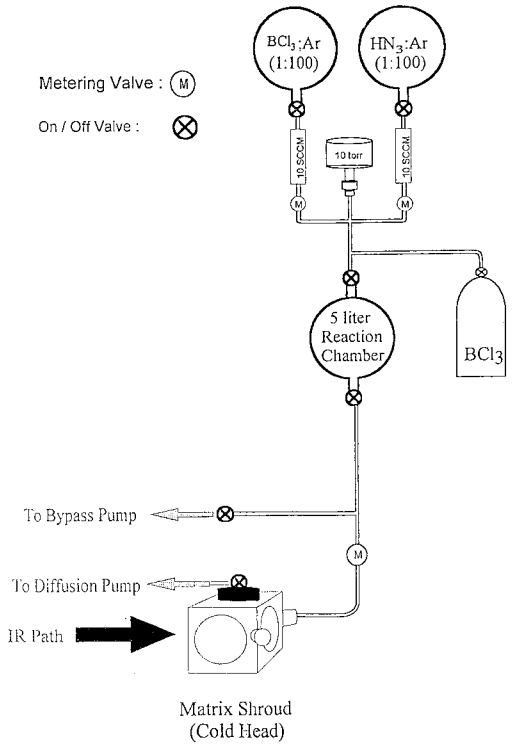

Figure 1. $B(N_3)_3$ generator coupled to the low-temperature matrix isolation apparatus. See text for an explanation.

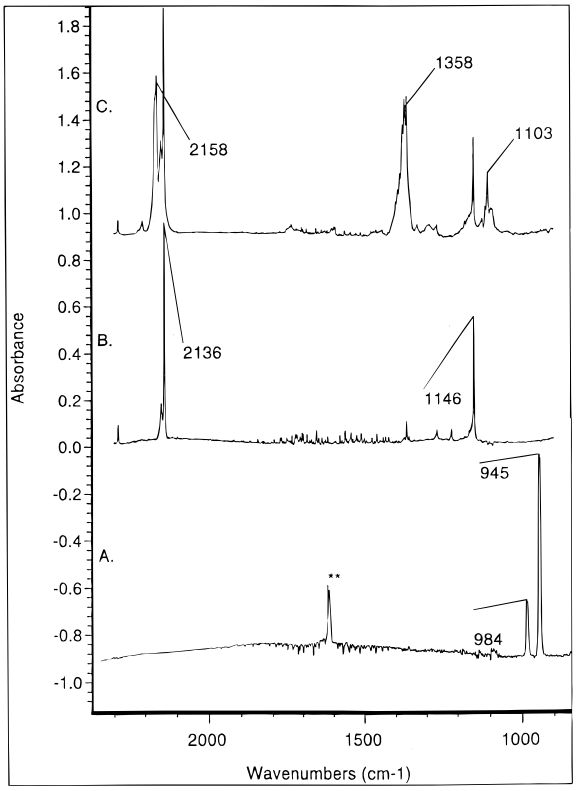

Figure 2. FTIR spectra of low-temperature argon matrixes containing (A) BCl_3, (B) HN_3, and (C) $B(N_3)_3$ with excess HN_3. The ν in wavenumbers for the major peaks of each molecule is labeled. A double asterisk denotes the presence of water in the matrix.

to the manifold. Downstream of each bulb was a 10 sccm flow meter and a stainless steel metering valve used to monitor and control the gas flows. Typical flows were around 2 and 6 sccm for the BCl_3/Ar and the HN_3/Ar, respectively. The BCl_3/Ar and HN_3/Ar mixtures were combined and passed through a 5 L Pyrex mixing bulb, providing a 10 min reaction time and good yields of $B(N_3)_3$ in these experiments. The pressure in the synthesis manifold was controlled by throttling the on/off valve on the manifold vacuum pump which was attached downstream of the 5 L mixing bulb. A metering valve was also located downstream of the mixing bulb to allow a small percentage of the gas mixture to be admitted to the cold head for deposition. It was necessary to passivate the entire synthesis manifold with pure BCl_3 prior to carrying out the synthesis if the system had been exposed to air, and for this purpose, a stainless steel gas bottle of pure BCl_3 (gas, 400 Torr) was also attached to the manifold.

In a typical experiment, the system was passivated, if necessary, with a few Torr of pure BCl_3. The pressure in the system rises during the passivation process due to reactions of BCl_3 with water adsorbed on the walls of the system. The passivation was judged to be completed when the pressure stopped increasing. The system was then pumped out and the synthesis started by setting the stoichiometric flows of the reagent gases. The pressure in the manifold was set between 5 and 10 Torr, and the stainless steel metering valve on the cryostat was opened to admit a small flow of the product mixture for deposition on the cold (10 K) KCl window mounted in the cryostat. The cold head was positioned in the sample chamber of the Nicolet 5DXPC FTIR spectrometer (resolution ± 2 cm^{-1}) so that the IR beam passed through the cold KCl window. A typical deposition was carried out for about 1 h, after which the matrix was photolyzed with the loosely focused output of a D_2 lamp. The progress of the deposition and of the photolysis was monitored via the IR spectrum.

Calculations were performed with Gaussian 94 on either an IBM model 250 RS6000 or a Silicon Graphics Octane workstation.[13]

Results and Discussion

Infrared Spectrum of $B(N_3)_3$/Ar Matrix. Figure 2 shows the IR spectra of BCl_3 (curve A) and of HN_3 (curve B) in low-temperature matrices prepared with 1% mixtures of each gas in argon. Curve C of Figure 2 shows the IR spectrum of a matrix generated when the 1% mixtures of HN_3 and BCl_3 in argon were combined in the gas manifold system prior to deposition with a somewhat larger than 3 to 1 flow ratio. Excess HN_3 is indicated in curve C by the features at 2136 and 1146 cm^{-1}.[14] The BCl_3 peaks around 950 cm^{-1} are not present in curve C, indicating that all of the BCl_3 had reacted.[15] The maxima at 2158, 1358, and 1103 cm^{-1} in the curve C spectrum are not in either the HN_3 or the BCl_3 argon matrix spectra, the appearance of these features depended on the presence of HN_3 and BCl_3 at a minimum flow ratio of 3 to 1, and, as is discussed below, all of these peaks decreased at the same rate upon photolysis. The relative intensities and the positions of these bands compare well with the features reported[1] in the gas-phase IR spectrum of $B(N_3)_3$ at 2163, 1360, and 1100 cm^{-1} and are therefore assigned to $B(N_3)_3$ in a low-temperature argon matrix. Although $B(N_3)_3$ has many more than three vibrational modes that are infrared-active, because of its symmetry, only three modes induce a sufficient change in the dipole moment to have observable infrared intensity in the 400$-$4000 cm^{-1} range of our FTIR spectrometer.

Calculations of the vibrational frequencies of the ground electronic state of $B(N_3)_3$ were reported as a part of the gas phase work of ref 1. These calculations were expanded (with

TABLE 1: Observed and Calculated Frequencies (cm^{-1}) for the Observable Infrared Transitions of $B(N_3)_3$

	ν_{17}/ν_{18}	$\nu_{20}\nu_{21}$	ν_{22}/ν_{23}
gas phase[a]	1100	1360	2163
Ar matrix (this work)			
$^{11}B(N_3)_3$	1103	1358[b]	2158
$^{10}B(N_3)_3$	1120[c]	1371	
difference	17	23	
calculations [MP2/6-31G(d)]			
$^{11}B(N_3)_3$[a]	1146	1451	2202
$^{10}B(N_3)_3$ (this work)	1167	1476	2202
difference	21	25	

[a] From ref 1. [b] This is the frequency of one of the three observed matrix sites. [c] This assignment is tentative because of the low signal-to-noise ratio for this feature.

Gaussian 94)[13] as a part of this study to include the boron isotope ^{10}B, and the results (Table 1) predict that isotopic separations large enough to be seen in low-temperature matrix spectra exist for two of the three observable vibrational modes. The natural isotopic abundances of ^{11}B and ^{10}B are 80% and 20%, respectively, so the ratio of the ^{11}B to ^{10}B vibrational features will be 4:1.

Expanded views of the $B(N_3)_3$ infrared spectrum are shown in Figure 3. The 2100−2200 cm^{-1} region (Figure 3A) shows the $B(N_3)_3$ peak at 2158 cm^{-1} and the HN_3 peak at 2136 cm^{-1}. Strong infrared absorptions in this region are characteristic of azide-containing molecules and are due to the asymmetric N_3 stretch.

The BN stretching region (Figure 3B) shows a "red" series of three peaks at 1358, 1365, and 1371 cm^{-1} and a lower intensity "blue series" series of three peaks at 1380, 1387, and 1394 cm^{-1}. Although the relative heights of the peaks within each series varied from matrix to matrix, when the 1358 cm^{-1} peak was the most intense of the red series, the 1380 cm^{-1} peak was the most intense of the blue series. Similarly, the intensities of the 1365 and 1387 cm^{-1} peaks and of the 1371 and 1394 cm^{-1} peaks tracked together. For these pairs of peaks (i.e., 1358 and 1380 cm^{-1}, 1365 and 1387 cm^{-1}, 1371 and 1394 cm^{-1}), the peak separation averaged 22 cm^{-1}, and the intensity ratio of the red member to the blue member was approximately 4:1. The calculations of the boron-10 isotope vibrational frequencies predict a 25 cm^{-1} isotope shift for this mode; thus, the 1358−1380, 1365−1387, and 1371−1394 cm^{-1} peak pairs are assigned as the $^{11}B-^{10}B$ isotope peaks for the BN stretch. These groups of peaks appeared in many of the $B(N_3)_3$/Ar matrixes prepared, although in a few matrixes, only the 1371 and 1394 cm^{-1} peaks appeared. These data are indicative of three $B(N_3)_3$ matrix sites in our argon matrices.

Figure 3C shows the $B(N_3)_3$ and HN_3 peaks at 1103 and 1146 cm^{-1}, respectively. These features are also characteristic of azide-containing molecules and are usually referred to as the N_3 symmetric stretch. Upon examination of these vibrational modes with the program AniMol[16] (which animates the normal modes calculated with Gaussian94), the motion in HN_3 is seen to consist of the $HN-N_2$ stretch coupled with the $H-N-N_2$ bend. The motion in the $B(N_3)_3$ mode is very similar with a $\sim BN-N_2$ stretch coupled to the $B-N-N_2$ bend, in the plane of the molecule. In the case of $B(N_3)_3$, the fact that there is significant motion of the B atom implies that a second peak corresponding to the ^{10}B isotope should appear shifted to higher frequencies in the spectrum. The calculations (see Table 1) predict a boron isotope shift of 22 cm^{-1}, so, assuming a scaling factor of unity, the ^{10}B isotope peak should appear at 1125 cm^{-1} with one-fourth the intensity of the 1103 cm^{-1} peak. The 1103 cm^{-1} peak has an absorbance of 0.056, so the isotope peak at 1125 cm^{-1} would have an absorbance of 0.014. There is a weak feature around 1120 cm^{-1} with a 0.012 absorbance that may well be the ^{10}B isotopic peak. The peak that appears at 1111 cm^{-1} is too intense and not shifted far enough to the blue to be the ^{10}B isotope peak; however, it decreases at the same rate as the 1103 cm^{-1} peak upon photolysis and is likely the N_3 "symmetric stretch" of $B(N_3)_3$ in a different matrix site.

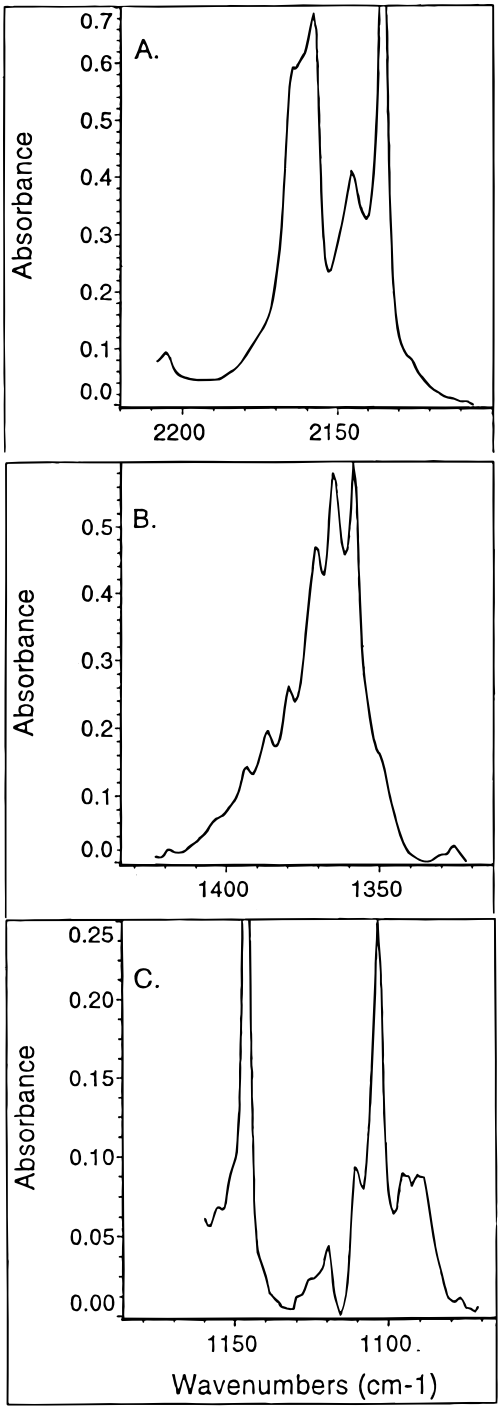

Figure 3. Expanded regions of the FTIR spectrum in Figure 2C: (A) the "N_3 asymmetric" stretching region from 2100 to 2220 cm^{-1}; (B) the BN stretching region from 1310 to 1435 cm^{-1}; (C) the "N_3 symmetric" stretching region from 1065 to 1190 cm^{-1}.

Photolysis of $B(N_3)_3$. The same three regions of the IR spectrum of a $B(N_3)_3$/argon matrix as shown in Figure 3 are presented in Figure 4 as a function of photolysis time with the D_2 lamp. In Figure 4A, the 2100−2200 cm^{-1} region, the decrease of the $B(N_3)_3$ band at 2158 cm^{-1}, and the growth of a

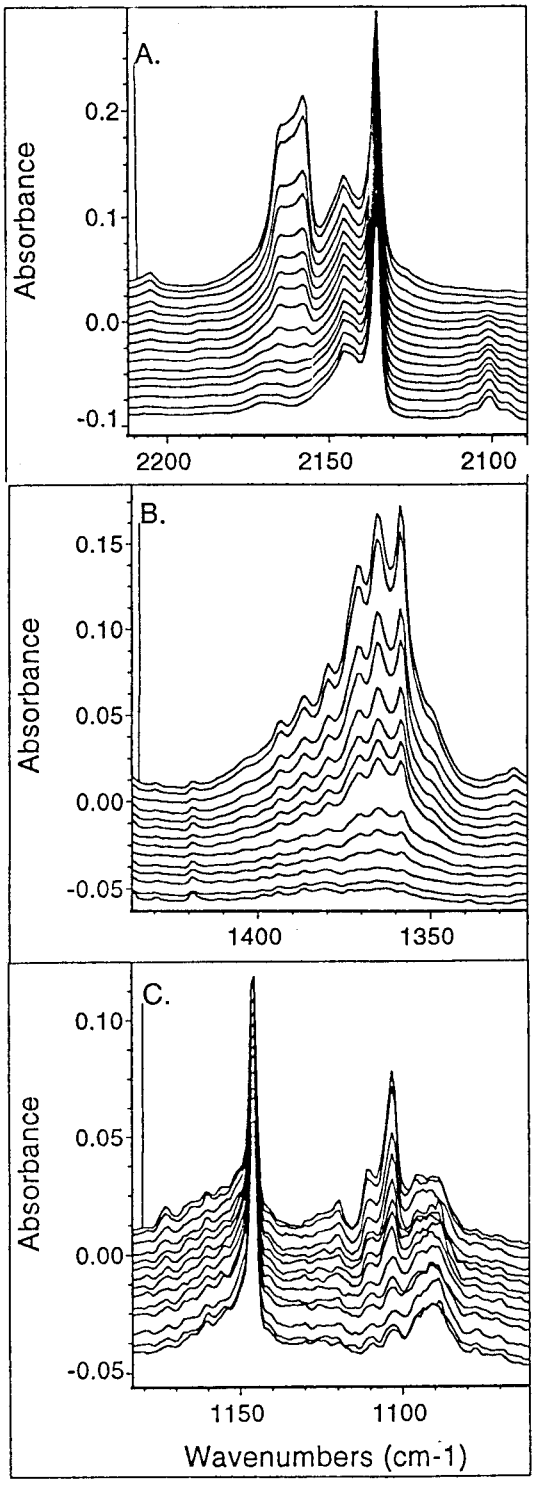

Figure 4. Same expanded regions of the FTIR spectrum from Figure 3 showing the changes that occurs as the $B(N_3)_3$/Ar matrix is photolyzed. The top spectrum is before photolysis, and the bottom spectrum is after 2 h of UV photolysis in each case. (A) The "N_3 asymmetric" stretching region from 2100 to 2220 cm^{-1}. (B) The BN stretching region from 1310 to 1435 cm^{-1}. (C) The "N_3 symmetric" stretching region from 1065 to 1190 cm^{-1}.

small peak at 2100 cm^{-1} are apparent. In the B−N stretching region (Figure 4B), the ^{11}B "red" series and the ^{10}B "blue" series of peaks decrease in concert, supporting the assignment of these features to three matrix sites. Figure 4C shows the 1050−1200 cm^{-1} region. The peaks at 1103 and 1111 cm^{-1} decrease together and so does the very weak feature at 1120 cm^{-1}. The maximum to the red of the 1103 cm^{-1} does not decrease during

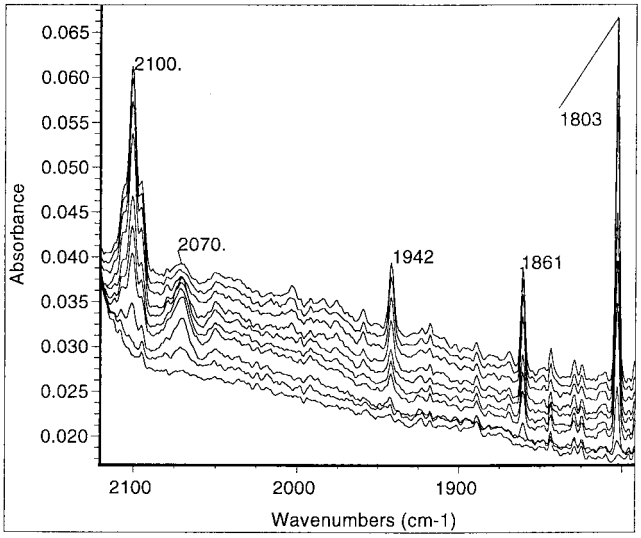

Figure 5. The 1800−2120 cm^{-1} region of the FTIR spectrum showing the peaks at 2100, 1942, 1861, and 1803 cm^{-1} growing in as a function of photolysis time. The bottom spectrum is the region before photolysis, and the top spectrum is the region after 2 h of UV photolysis.

the photolysis and is therefore not associated with $B(N_3)_3$. There is also a small decrease in the HN_3 peaks at 2136 and 1146 cm^{-1}. The growth of features at 2100, 1942, 1861, and 1803 cm^{-1} are observed as a function of photolysis time as shown by the spectra in Figure 5. One additional feature at 2070 cm^{-1} is observed to grow during the first part of the photolysis and then gradually disappear. This behavior is distinct from that of the other four peaks and is assumed to be due to a photolytically unstable product.

In Figure 6A, peak height vs photolysis time is plotted for the $B(N_3)_3$ peaks at 2158, 1358, and 1103 cm^{-1} and for the HN_3 peak at 2136 cm^{-1}. The $B(N_3)_3$ peaks decay rapidly in an exponential manner, whereas the HN_3 peak shows a much slower decay rate. A plot of the normalized peak heights vs photolysis time (Figure 6B) shows even more clearly that the $B(N_3)_3$ peaks decay at the same rate (the points are virtually on top of each other), much faster than the HN_3 decay. When these curves are fit with an exponentially decaying function, the decay constants listed in Table 2 are obtained. The three $B(N_3)_3$ peaks are seen to decrease with an average decay constant of 7.0×10^{-4} s^{-1}, and the HN_3 peak decays with a much slower rate of 6.3×10^{-5} s^{-1}. The growth behavior of the new features is shown in Figure 7. Figure 7A shows the plot of peak height vs photolysis time, and Figure 7B shows the normalized peak heights vs photolysis time. It is apparent that the 2100, 1861, and 1802 cm^{-1} peaks grow at the same exponential rate, and when these curves are fit with an exponentially rising function, the average growth constant is found to be 5.6×10^{-4} s^{-1}, whereas the 1942 cm^{-1} growth is slower with a growth constant of 3.4×10^{-4} s^{-1}. Consequently, the 1942 cm^{-1} feature is assigned to a separate species. The relative integrated intensities of the remaining three peaks at 2100, 1861, and 1803 cm^{-1} are 1.00, 0.16, and 0.63, respectively. The values in Table 2 indicate that the growth rate for the 2100, 1861, and 1803 cm^{-1} features is somewhat slower than the decay rate of the $B(N_3)_3$ peaks, suggesting a loss mechanism. Since the matrix was continuously irradiated with the D_2 lamp, it is quite likely that the product is being slowly photolyzed.

In work done by Andrews et al.,[10] in which several B_xN_y species were trapped in low-temperature argon matrixes, the linear molecule NNBN was identified on the basis of its infrared spectrum, isotopic data, and ab initio calculations. Table 3 lists

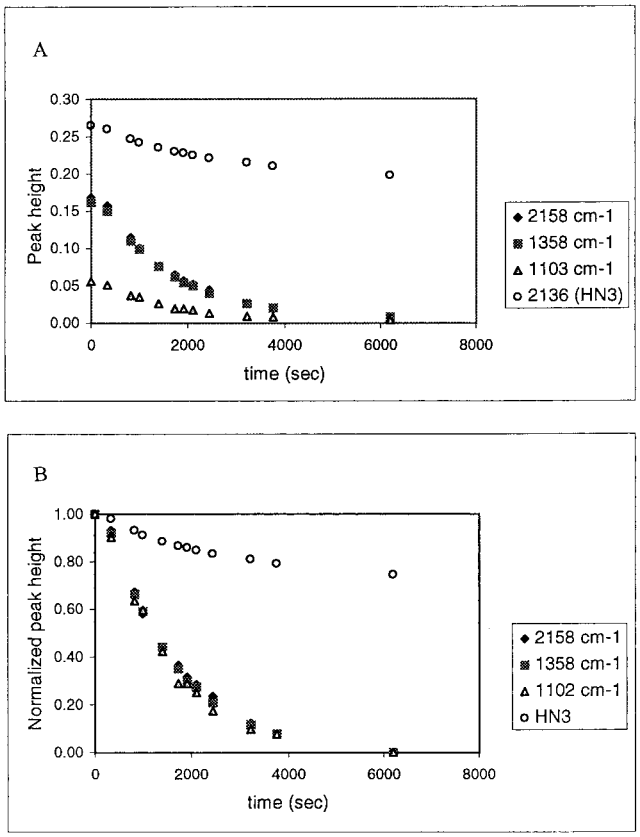

Figure 6. (A) IR absorbance for the $B(N_3)_3$ peaks and one of the HN_3 peaks as a function of photolysis time. (B) The same data as in (A), but showing normalized IR absorbance as a function of photolysis time. The HN_3 peak displays a much slower photolysis rate than do the $B(N_3)_3$ peaks.

TABLE 2: Decay Rate Constants (s^{-1}) and Growth Rate Constants Obtained from Exponential Fits to the Data Shown in Figures 2−4

	IR freq, cm^{-1}	rate constants
decaying IR bands	2158	6.8×10^{-4}
	1358	7.0×10^{-4}
	1102	7.3×10^{-4}
	2146 (HN_3)	6.3×10^{-5}
growing IR bands	2100	5.3×10^{-4}
	1861	5.8×10^{-4}
	1803	5.7×10^{-4}
	1942	3.4×10^{-4}

the frequencies and relative intensities reported by Andrews' group for NNBN and the same data for the product peaks observed in the $B(N_3)_3$ matrix photolysis. The mode assignments are based on isotopic studies done by Andrews' group. The 760.3 cm^{-1} peak was reported by Andrews et al. to have a low relative intensity and could not be seen in our spectra. The noise in the 700−800 cm^{-1} region of our spectrum was 0.005 absorbance units, so the integrated intensity for this mode relative to the strongest peak at 2100 cm^{-1} (which has an integrated absorbance of 0.19 in the spectrum of Figure 5) cannot be larger than 0.03. There is good agreement between the remaining three peaks at 2091.7, 1802.0, and 1859.6 cm^{-1} from Andrews work and the three peaks at 2100, 1803, and 1861 cm^{-1} in this work. The 8 cm^{-1} difference for the highest frequency mode (the N−NBN stretch) is likely the result of different matrix site characteristics. The Andrews group reported that, in a N_2 matrix, the N−NBN and NNB−N stretching fundamentals are at 2125 and 1806 cm^{-1}, respectively, blue-shifted relative to the argon matrix values.[11] Our values

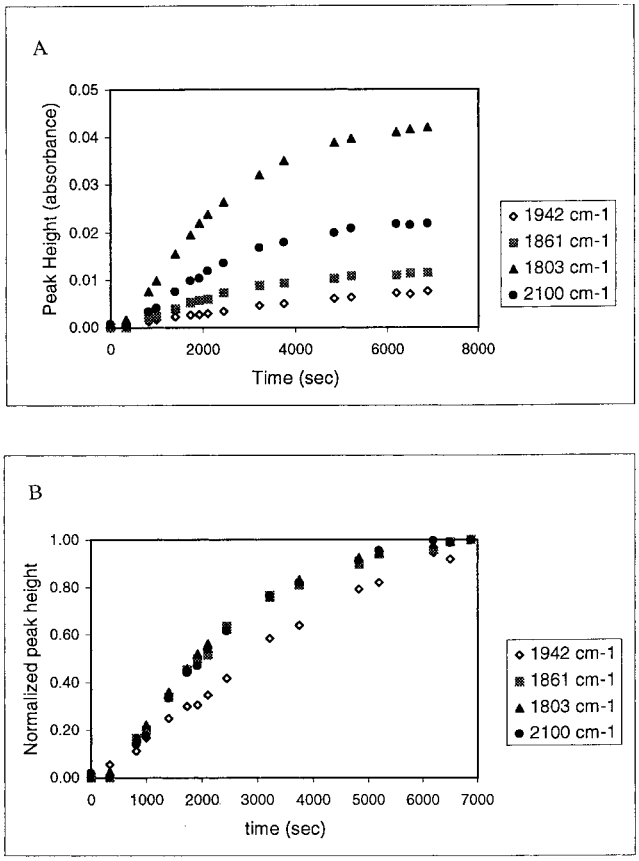

Figure 7. (A) IR absorbance for the new peaks appearing between 1800 and 3120 cm^{-1} as a function of photolysis time. (B) Same data as in (A), but showing normalized IR absorbance as a function of photolysis time. The 1942 cm^{-1} shows different growth behavior for the other peaks at 2100, 1861, and 1803 cm^{-1}.

TABLE 3: Assignments and Comparisons of the Infrared Features (in cm^{-1}) Observed and Calculated for NNBN

vibration	published[a]	this work	CCSD(T) 6-311G*
$^{11}B-^{14}N$ stretch (ν_2)	1802.0	1803 ± 2	1823.2
$^{10}B-^{14}N$ stretch (ν_2)	1859.6	1861	1883.9
$^{14}N-^{14}N$ stretch (ν_1)	2091.7	2100	2117.3
$^{14}N-^{11}B$ stretch (ν_3)	760.3	*b*	760.3

[a] Data from ref 10. [b] This weak feature was not observable in our spectrum.

of 2100 and 1803 cm^{-1} for the N−NBN and NNB−N stretches are intermediate between the argon and nitrogen matrix values. This reflects the fact that in our work the NNBN molecule share the matrix site with three N_2 molecules also generated in the photolysis, producing an effective mixed Ar/N_2 cage for the NNBN. The shoulders that appear on each side of ν_1 in this work are likely due to the effect of different matrix sites.

Although NNBN is isoelectronic with both cyanogen (NCCN) and isocyanogen (CNCN), there are analogies between NNBN and isocyanogen that do not exist for cyanogen. NNBN has a permanent dipole moment and two different B−N bonds. Likewise, isocyanogen has a permanent dipole moment and has two different C−N bonds. Cyanogen, on the other hand, has no permanent dipole moment, and the C−N bonds are identical. An NBO charge distribution analysis gives the distributions indicated in Table 4, and NNBN and CNCN display alternating charge distributions. The similarity between NNBN and CNCN leads to the expectation that the IR spectra of NNBN and CNCN will be similar. The CNCN spectrum, reported as part of a low-temperature matrix isolation study of the products of

TABLE 4: Charge Distributions from an NBO Analysis (B3PW91/6-311G*) for NNBN, CNCN, and NCCN

NNBN	CNCN	NCCN
N −0.48	N −0.25	N −0.18
B +0.38	C +0.42	C +0.18
N −0.07	N −0.58	C +0.18
N +0.18	C +0.41	N −0.18

TABLE 5: Calculated and Observed Vibrational Frequencies and Intensities for NNBN[a]

ν	scaled HF 6-311G*[b]	MP2 6-311G*	CCSD(T) 6-311G* ^{11}B isotope	CCSD(T) 6-311G* ^{10}B isotope
7	154.7 (17)	171.5 (15)	149.1	152.6
6	154.7 (17)	171.5 (15)	*c*	*c*
5	466.2 (4)	502.0 (0.5)	465.3	368. 5
4	466.2 (4)	502.0 (0.5)	469.4	475.4
3	638.9 (45)	789.9 (0.1)	760.4	764.3
2	1928.3 (68)	1563.7 (2151)	1823.2	1883.9
1	2407.4 (177)	1734.1 (195)	2117.3	2117.4

[a] The frequencies are in cm^{-1}; the calculated intensities in parentheses are in units of km/mol. [b] The Hartree−Fock frequencies were scaled by 0.89. [c] Since the optimized geometry was not precisely linear (angle 179.9°), the doubly degenerate ν_6 and ν_7 modes appeared as a single bending mode.

thermolysis of norbornadienone azine,[17] shows three peaks, the ν_1, ν_2, and ν_3 modes. The relative peak heights in the CNCN argon matrix spectrum from ref 17 are 0.63, 1.00, and 0.05 for ν_1, ν_2, and ν_3, respectively. The peak heights in the spectrum of NNBN are very similar with $\nu_1{:}\nu_2{:}\nu_3 = 0.68{:}1.00{:}\leq 0.03$.

Prior to this work, computational efforts on NNBN consisted of an ab initio study of bonding trends in the 26-electron ABCD systems by Pyykko and Runeberg,[18] at the Hartree−Fock and MP2 levels of theory with the 6-31G* basis set, and Hartree−Fock calculations of the ground-state vibrational frequencies by Andrews et al.[10] Although the HF frequencies (scaled by 0.89) do not agree particularly well with the experimentally observed frequencies for NNBN, isotopic shifts for the ^{10}B and ^{15}N isotopomers are well-predicted. As a part of this study, the results of calculations at the MP2, diffuse functional theory (B3PW91), coupled clusters with double excitations (CCD), and coupled clusters with single, double, triple excitations [CCSD(T)] levels of theory with the 6-311G* basis set were explored. The HF, MP2, and CCSD(T) results are listed in Tables 5 and 6, and it is not surprising that the best frequencies were obtained with CCSD(T). There is 1% or less deviation between the CCSD(T)/6-311G* frequencies and the experimental frequencies, and the calculated ^{10}B isotope shift for ν_2 agrees well with the observed shift. (While it is common for a larger basis set to be used with the CCSD(T) level of theory, in this case, the additional computational time does not seem justified or necessary.) Frequency calculations for CNCN have been reported using the CCSD(T) method (with a basis set of 220 cGTOs),[19] and the agreement between the experimental values reported for CNCN in a low-temperature argon matrix is very good for this system as well.[17]

Because of the excellent agreement between the observed and CCSD(T) frequencies, the optimized CCSD(T) geometry is assumed to be close to the true geometry. The NNBN bond lengths from the HF, MP2, and CCSD(T) calculations are shown in Table 6. The MP2 results imply that the N−BNN and the NB−NN bonds are nearly equivalent, which is inconsistent with the observed IR spectrum (the two B−N bonds have very different stretching frequencies). While the HF calculation predicts a difference in the two B−N bond lengths, the N−NBN bond is predicted to be shorter than that observed for diatomic nitrogen (1.094 Å, and yet in the IR spectrum, the N−N bond frequency is significantly lower (2100 cm^{-1}) than that of diatomic nitrogen (2359.6 cm^{-1}).[20] The CCSD(T) geometry correctly predicts two different B−N bond lengths and that the N−NBN bond is longer that the N−N bond in diatomic N_2.

TABLE 6: Optimized Geometries for NNBN with Bond Lengths in angstroms and Energies in hartrees[a]

	HF 6-311G*	MP2 6-311G*	CCSD(T) 6-311G*
N−NBN	1.0722	1.1635	1.1300
NN−BN	1.4514	1.3657	1.4047
NNB−N	1.2223	1.3118	1.2820
energy	−187.964	−188.587	−187.910

[a] In all cases, the molecule was predicted to be linear within less than 0.01°.

Photolysis Mechanism. In the broad-band UV photolysis studies of the $B(N_3)_3$/Ar matrix, the dissociative 230 nm absorption band in $B(N_3)_3$ is clearly accessed. It is expected that this absorption leads to the breaking of the $\sim$N−N_2 bonds based on what is observed in other covalently bonded azides.[7−9] This would, however, leave a planar trigonal BN_3 fragment, not the linear NNBN that was observed in our photolysis experiments. The trigonal fragment was found to be stable as a singlet via Gaussian calculations, but the frequencies and relative intensities were completely inconsistent with those observed for the matrix photofragment (identified as NNBN above). It is still, however, possible that the trigonal BN_3 does form, that it is formed in a state with a higher multiplicity than a singlet, and that this state is not stable. If the initially formed state were dissociative along the N−B−N bend, it would lead to a rapid rearrangement to the NNBN molecule identified as the intermediate in this work. A potential surface calculation could address this issue.

The question then remains as to how the linear NNBN molecule leads to the formation of BN films. One proposal involves a "self-assembly" mechanism[21] in which the NNBN molecules align, such that a lone pair on the single terminal N of one NNBN is in position to be donated to the empty p orbital on the B atom of the neighboring NNBN. A third NNBN can then align with the second molecule, donating a lone pair to the B atom. Upon elimination of the N_2 groups, a hexagonal B_3N_3 molecule is produced, and empty orbitals are regenerated on the boron atoms. A sheet of such hexagons can be generated when more NNBN molecules align with these now empty orbitals. Cubic forms would require that the NNBN be energized in some way, for example, if one of the bending vibrations were excited significantly such that the geometry deviated from the linear structure or if the photolysis generated an excited electronic state of NNBN that is bent.

Conclusions

The first step in the mechanism for the photolytic decomposition of gaseous $B(N_3)_3$ proposed by Mulinax et al. predicted the formation of an intermediate BN_3 molecule, followed by the formation of BN films.[1] This work has shown that this intermediate is, in fact, the linear molecule NNBN and not the trigonal BN_3 fragment expected from the photolytic cleavage processes known to occur in other covalent azides. The formation of a BN film from linear NNBN molecules is proposed to occur via a "self-assembly" mechanism. Such a mechanism does appear to be more reasonable than what could be envisioned for the trigonal fragment. Based on the infrared frequencies of the B−N bonds in the starting materials and the final films, the formation of either h-BN or c-BN appears to be

more thermodynamically favorable if the starting material is linear NNBN rather than trigonal BN_3. The NN−BN bond is weaker than the BN bond in c-BN or the in-ring BN bonds in h-BN,[22] whereas the B−N bonds in a trigonal BN_3 are expected to be at least as strong as the c-BN or h-BN bonds if not stronger.

This work has interesting implications for the consideration of other novel chemical methods leading to the production of other interesting solids. In addition to using precursors that either contain the desired bonding arrangements or react to form them, one might look for precursors that are capable of "self-assembly" to generate the desired product. To this end, our work is continuing with a study of the partially azidified species, $BCl(N_3)_2$ and $BCl_2(N)_3$, and other group III azide species. Additional spectroscopic work on NNBN and on the photo-intermediates generated in these other azides is also underway.

Acknowledgment. This work was supported by the National Science Foundation under Grant CHE-9527080 and by the Air Force Office of Scientific Research under Grant F49620-97-1-0036. The authors also thank our colleague Robert D. Coombe for many useful discussions.

Note Added in Proof. CCSD(T) structure, energy, and frequency calculations using the DZP, cc-pVDZ, and TZ2P basis sets are available for NNBN[24] and are consistent with the calculations reported here.

References and Notes

(1) Mulinax, R. L.; Okin, G. S.; Coombe, R. D. *J. Phys. Chem.* **1995**, *99*, 6294.

(2) See for example: Synthesis & Properties of Boron Nitrides. In *Materials Science Forum*; Pouch, J. J., Allerevitz, A., Eds.; Aedermannsdorf: Switzerland, 1990; Vol. 54/55.

(3) Wentorf, Jr., R. H. *J. Chem. Phys.* **1962**, *36*, 1990.

(4) Saitoh, H.; Yarbrough, W. A. *Appl. Phys. Lett.* **1991**, *58*, 2482.

(5) Kester, D. J.; Messier, R. *Appl. Phys. Lett.* **1992**, *72*, 506.

(6) Qian, F.; Nagabushnam, V.; Singh, R. K. *Appl. Phys. Lett.* **1993**, *63*, 317.

(7) Patel, D; Pritt, Jr., A. T.; Benard, D. J. *J. Phys. Chem.* **1986**, *90*, 1931.

(8) MacDonald, M. A.; David, S. J.; Coombe, R. D. *J. Chem. Phys.* **1986**, *84*, 5513.

(9) Coombe, R. D.; Patel, D.; Pritt, Jr., A. T.; Wodarczk, F. J. *J. Chem. Phys.* **1981**, *75*, 2177.

(10) Andrews, L.; Hassanzadeh, P.; Burkholder, T. R.; Martin, J. M. L. *J. Chem. Phys.* **1993**, *98*, 922.

(11) Hassanzadeh, P.; Andrews, L. *J. Chem. Phys.* **1992**, *96*, 9177.

(12) Schlie, L. A.; Wright, M. W. *J. Chem. Phys.* **1990**, *92*, 394.

(13) Gaussian 94 (Revision A.1): Frisch, M. J.; Trucks, G. W.; Schlegel, H. B.; Gill, M. W.; Johnson, B. G.; Robb, M. A.; Cheeseman, J. R.; Keith, T. A.; Petersson, G. A.; Montgomery, J. A.; Raghavachari, K.; Al-Laham, M. A.; Zakrzewski, V. G.; Ortiz, J. V.; Foresman, J. B.; Cioslowski, J.; Stefanov, B. B.; Nanayakkara, A.; Challacombe, M.; Peng, C. Y.; Ayala, P. Y.; Chen, W.; Wong, M. W.; Andres, J. L.; Replogle, E. S.; Gomperts, R.; Martin, R. L.; Fox, D. J.; Binkley, J. S.; Defrees, D. J.; Baker, J.; Stewart, J. P.; Head-Gordon, M.; Gonzalez, C.; Pople, J. A. Gaussian, Inc., Pittsburgh, PA, 1995.

(14) Moore, C. B.; Rosen, K. *J. Chem. Phys.* **1966**, *44*, 4108.

(15) Clark, R. J. H.; Mitchell, P. D. *J. Chem. Phys.* **1972**, *56*, 2225. Dows, D. A.; Bottger, G. *J. Chem. Phys.* **1961**, *34*, 689.

(16) AniMol, Version 3.2, Innovative Software, Inc., 1995−96.

(17) Stroh, F.; Winnewisser, B. P.; Winnewisser, M.; Reisenauer, H. P.; Maier, G.; Goede, S. J.; Bickelhaupt, F. *Chem. Phys. Lett.* **1989**, *160*, 105.

(18) Pykko, P.; Runeberg, Nino, *J. Mol. Struct.* **1991**, *234*, 269.

(19) Botschwina, P.; Sebald, P. *Chem. Phys.* **1994**, *225*, 480.

(20) Herzberg, G. *Molecular Spectra and Molecular Structure I. Spectra of Diatomic Molecules*; Van Nostrand Reinhold: New York, 1950.

(21) Hout, R. F., Jr.; Levi, B. A.; Hehre, W. J. *J. Comput. Chem.* **1982**, *3*, 234.

(22) Private communications with Robert D. Coombe.

(23) Wells, A. F. *Structural Inorganic Chemistry*, 5th ed.

(24) Martin, J. M. L.; Slanina, Z.; Francois, J. P.; Gijbels, R. *Mol. Phys.* **1994**, *82*, 155.